

Current Biology

Intraspinal Sensory Neurons Provide Powerful Inhibition to Motor Circuits Ensuring Postural Control during Locomotion

Highlights

- CSF-contacting neurons are recruited during spontaneous tail muscle contractions
- CSF-contacting neurons project onto motor neurons and sensory interneurons of the escape circuit
- GABAergic synapses on these targets are large and depress with repetitive stimuli
- Silencing CSF-contacting neurons alters balance during fast locomotion

Authors

Jeffrey Michael Hubbard,
Urs Lucas Böhm, Andrew Prendergast,
Po-En Brian Tseng, Morgan Newman,
Caleb Stokes, Claire Wyart

Correspondence

claire.wyart@icm-institute.org

In Brief

Hubbard et al. demonstrate here that GABAergic sensory neurons, referred to as cerebrospinal fluid-contacting neurons, locally project onto the escape circuit within the spinal cord to control posture during active locomotion in the zebrafish larva.

Intraspinal Sensory Neurons Provide Powerful Inhibition to Motor Circuits Ensuring Postural Control during Locomotion

Jeffrey Michael Hubbard,^{1,2,3,4} Urs Lucas Böhm,^{1,2,3,4} Andrew Prendergast,^{1,2,3,4} Po-En Brian Tseng,^{1,2,3,4} Morgan Newman,⁵ Caleb Stokes,^{1,2,3,4} and Claire Wyart^{1,2,3,4,6,*}

¹Institut du Cerveau et de la Moelle Épine, Hôpital Pitié Salpêtrière, 47 Boulevard de l'Hôpital, 75013 Paris, France

²INSERM UMRS 1127, 75013 Paris, France

³CNRS UMR 7225, 75005 Paris, France

⁴UPMC University Paris 06, 75005 Paris, France

⁵Department of Genetics and Evolution, School of Biological Sciences, The University of Adelaide, Adelaide, SA 5005, Australia

⁶Lead Contact

*Correspondence: claire.wyart@icm-institute.org

<http://dx.doi.org/10.1016/j.cub.2016.08.026>

SUMMARY

In the vertebrate spinal cord, cerebrospinal fluid-contacting neurons (CSF-cNs) are GABAergic neurons whose functions are only beginning to unfold. Recent evidence indicates that CSF-cNs detect local spinal bending and relay this mechanosensory feedback information to motor circuits, yet many CSF-cN targets remain unknown. Using optogenetics, patterned illumination, and *in vivo* electrophysiology, we show here that CSF-cNs provide somatic inhibition to fast motor neurons and excitatory sensory interneurons involved in the escape circuit. Ventral CSF-cNs respond to longitudinal spinal contractions and induce large inhibitory postsynaptic currents (IPSCs) sufficient to silence spiking of their targets. Upon repetitive stimulation, these IPSCs promptly depress, enabling the mechanosensory response to the first bend to be the most effective. When CSF-cNs are silenced, postural control is compromised, resulting in rollovers during escapes. Altogether, our data demonstrate how GABAergic sensory neurons provide powerful inhibitory feedback to the escape circuit to maintain balance during active locomotion.

INTRODUCTION

Cerebrospinal fluid-contacting neurons (CSF-cNs) were first identified nearly a century ago and are highly conserved in the spinal cord, having been described in over 200 vertebrate species [1, 2]. Despite being a central element of the vertebrate spinal cord, the precise cellular connectivity and function of CSF-cNs have only recently begun to be described [3–7]. CSF-cNs exhibit an apical dendritic extension bearing microvilli situated in the lumen of the central canal. These cells express the channel transient receptor potential polycystic 3 (TRPP3 or

polycystic kidney disease 2-like 1; PKD2L1) [8, 9], allowing them to respond to variations in pH and osmolarity in the CSF [4, 8, 10]. Based on their anatomy, these cells have been proposed to detect flow or content of the CSF [11].

Recently, we demonstrated that dorsal CSF-cNs on either side of the central canal are activated by curvature of the spinal cord selectively on the side of bending in larval zebrafish [7]. We showed evidence that CSF-cNs modulate stereotyped behaviors in intact zebrafish thought to be driven by locomotor central pattern generators (CPGs), both for slow locomotion [5] as well as for fast locomotion during acoustic escapes [7]. However, precise cellular connections by which CSF-cNs modulate fast locomotion have not been previously investigated. Escapes in fish are a stereotyped movement program that is typically triggered by the sequential activation of sensory neurons, leading to recruitment of the Mauthner cell in the hindbrain [12, 13] and finally the activation of spinal neurons, including primary motor neurons. This induces a large C bend on one side of the animal that is coincident with recruitment of commissural inhibitory glycinergic interneurons to silence motor output on the other side [14, 15]. The neurons that underlie locomotion are known to reside in the ventral spinal cord, where CSF-cNs send most of their projections [3, 5, 11]. This places CSF-cNs in an optimal position to modulate the spinal escape circuit. To establish the postsynaptic targets of CSF-cNs within the spinal cord, we combined whole-cell patch-clamp recordings of putative targets with two-dimensional (2D) light patterning and channelrhodopsin (ChR2)-mediated activation of CSF-cNs in the zebrafish larva. We took advantage of transgenic lines labeling specific classes of spinal neurons in order to target the recordings to given cell types, whose identity was later confirmed by cell filling and morphological reconstruction.

Here we provide evidence that ventral CSF-cNs are recruited during spontaneous contraction of the animal involving a longitudinal bend. We show that these CSF-cNs innervate multiple components of the escape circuit, namely a subset of primary motor neurons as well as a class of glutamatergic interneurons involved in sensory motor gating. We found that this connectivity with key elements of the escape circuit is specific, because

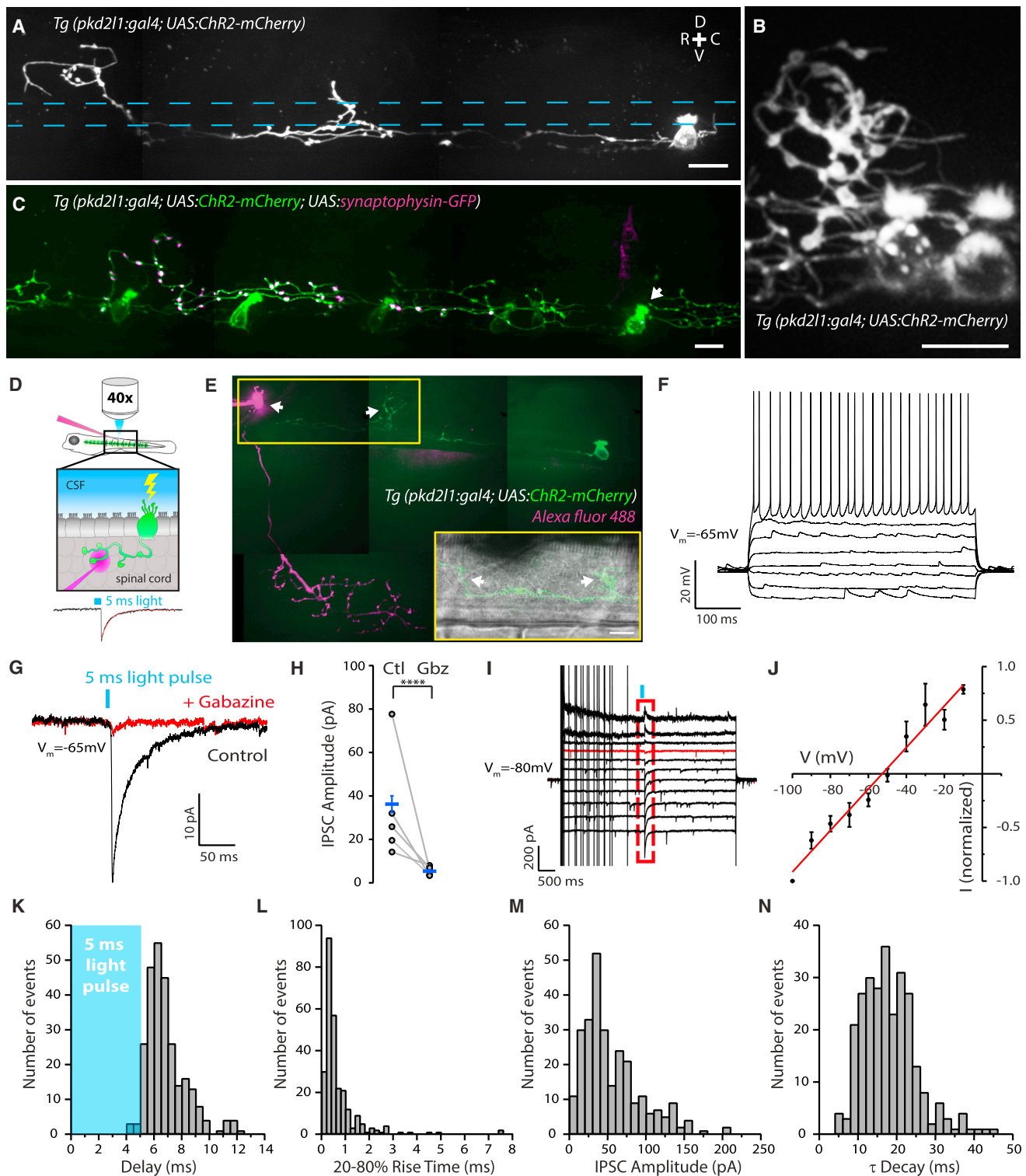


Figure 1. CSF-cNs Specifically Innervate the CaP Motor Neuron

(A) Z projection stack showing a single ventral CSF-cN in a *Tg(pkcd211:gal4; UAS:ChR2-mCherry)* double-transgenic larva at 3 days post-fertilization (dpf). Top right: dorsal (D), ventral (V), rostral (R), and caudal (C) orientation indicated by the cross. The central canal location is indicated by blue dashed lines.

(B) CSF-cN axons and varicosities in the 3-dpf *Tg(pkcd211:gal4; UAS:ChR2-mCherry)* transgenic larva surround a dorsal cell body.

(C) Labeling of putative presynaptic boutons originating from a single CSF-cN (arrow) expressing synaptophysin-GFP in a 4-dpf *Tg(pkcd211:gal4; UAS:ChR2-mCherry)* transgenic larva after injection of the construct *UAS:synaptophysin-GFP*.

(legend continued on next page)

CSF-cNs did not project onto either glycinergic premotor interneurons or mechanosensory neurons involved in the escape response. Ventral CSF-cNs provide somatic, perisomatic, and axon initial segment innervation to primary motor neurons, reminiscent of basket cell synapses. The innervation of the motor neuron pool by CSF-cNs is selective for caudal primary motor neurons referred to as CaP motor neurons, which are involved in fast locomotion and postural control [16, 17]. The innervation of sensory interneurons is restricted to the initial segment and soma, with occasional axo-dendritic contacts. On both of these CSF-cN targets, ventral CSF-cNs induce a remarkably large and reliable inhibitory postsynaptic current (IPSC) with similar properties. Stimulus trains at moderate frequencies (10–20 Hz) rapidly induce short-term depression of the postsynaptic response. Spatially restricted photoactivation of single CSF-cNs indicates that multiple CSF-cNs converge onto a given target. The convergence of inputs onto single primary motor neurons from ventral CSF-cNs provides strong GABAergic inhibition capable of efficiently silencing motor output. Furthermore, we show behaviorally that silencing CSF-cN output with botulinum toxin results in a defect in postural control during acoustically induced escape responses.

Our findings demonstrate that an intraspinal GABAergic system actively senses spinal cord curvature during locomotion and constitutes a local sensory-motor loop that modulates posture during rapid movement.

RESULTS

Dorsal Projections from Ventral CSF-cNs Innervate Primary Motor Neurons

In order to identify CSF-cN targets, we carefully investigated the morphology of their axonal projections. Although a large density of CSF-cN axons project within the ventral portion of the spinal cord [5], some of the ventral CSF-cNs extend axonal projections dorsally, encircling large cell bodies (Figures 1A–1C and 1E). This structure contained multiple large varicosities (Figures 1A and 1B) associated with putative presynaptic boutons labeled by synaptophysin-GFP (Figure 1C). The position of these presynaptic structures suggested innervation of dorsal primary motor

neurons (pMNs), which are recruited during escapes and fast swimming in zebrafish larvae [17]. We screened different transgenic cell lines labeling specific cell types in the zebrafish spinal cord and identified the anatomical contact of CSF-cNs to the caudally located dorsal primary motor neurons known as CaP [18].

Selective Connectivity to Primary Motor Neurons Involved in Fast Locomotion and Postural Control

To test the functional connectivity of CSF-cNs to primary motor neurons, we optically activated CSF-cNs expressing ChR2 while recording from the cell body surrounded by presynaptic boutons (Figure 1D). Cells whose somas were encircled by the CSF-cN basket structure correspond to CaP motor neurons, as shown by their characteristic morphology after dye filling (Figure 1E), input resistance, and sustained firing of action potentials at high frequency (Figure 1F). The morphology of the axonal projection suggests that individual CSF-cNs innervate multiple CaP motor neurons along the rostro-caudal axis (Figure 1E). In our conditions, a 5-ms light pulse typically induces a single spike in CSF-cNs expressing ChR2-mCherry (see [5]). Following the optical activation of CSF-cNs, we recorded large IPSCs in CaP motor neurons occurring without failure (34 out of 34 CaP motor neurons recorded). These IPSCs were abolished by bath application of the GABA_A receptor antagonist gabazine (Figures 1G and 1H). The light-induced current-voltage relationship showed that the IPSCs reversed around –53 mV, close to the calculated reversal potential of chloride in our conditions (E_{Cl} –51 mV; Figures 1I and 1J). The timing and kinetics of the light-induced IPSCs were consistent with monosynaptic currents mediated by GABA_A receptors (Figures 1K–1N). These data indicate that CaP motor neurons are one major target of CSF-cNs.

Other Motor Neurons Are Minimally Innervated by CSF-cNs

Given the significant innervation pattern observed for CaP motor neurons, we proceeded to determine whether other motor neurons (both primary and secondary) receive synaptic input from CSF-cNs. Targeted whole-cell recordings of primary and secondary motor neurons were performed in *Tg(parg^{mn2}-GFP)*

(D) Schematic of the experimental paradigm used for ChR2-mediated mapping of connectivity illustrates a CSF-cN expressing ChR2-mCherry (green) illuminated by a short pulse of light and the whole-cell patch-clamp recording of the target neuron with a pipette containing the Alexa dye to confirm the nature of the cell type (top). A 5-ms light pulse is sufficient to induce a single spike reliably in CSF-cNs (see [5]), and the subsequent IPSC is recorded in the target neuron (bottom).

(E) Z projection stack showing a CaP motor neuron filled with the Alexa dye (magenta) innervated by a single CSF-cN (green) in a 4-dpf *Tg(pkcd2l1:gal4; UAS:ChR2-mCherry)* transgenic larva with sparse expression of ChR2. The boxed region shows a wide-field image with the CaP cell body contacted by the axonal projection of the labeled CSF-cN. Arrows indicate the dorsal projections that surround the soma of the CaP motor neuron recorded and filled as well as another putative CaP motor neuron in the adjacent caudal segment.

(F) Current-clamp recording of a typical CaP motor neuron showing phasic action potential firing in response to current injection (steps of 20 pA from –50 pA to +90 pA).

(G) Voltage-clamp recording from a CaP motor neuron ($V_m = -65$ mV) showing evoked IPSCs following 5-ms light pulses before (black trace; average of ten trials) and after 10 μ M gabazine treatment (red trace; average of ten trials).

(H) Summary data showing that the IPSCs are abolished by gabazine. Each experiment (circle) is the average of ten trials before (Ctl) and after gabazine (Gbz) treatment (mean amplitude of control IPSC, 36.2 ± 24.9 pA; mean amplitude of gabazine IPSC, 5.4 ± 4.1 pA; $n = 5$, **** $p < 0.0001$).

(I and J) Voltage steps and corresponding current-voltage (I–V) curve indicate that the IPSCs (within the red dashed box) reverse at –53 mV (red trace in I) close to the reversal potential of chloride (E_{Cl} –51 mV) in our recording conditions ($n = 6$ cells).

(K–N) Distribution of IPSC delay (K; mean 6.86 ± 0.09 ms), 20%–80% rise time (L; mean 0.89 ± 0.19 ms), current amplitude (M; mean 55.19 ± 2.34 pA, corresponding to a conductance of 3.94 nS), and time decay τ (N; mean 18.04 ± 0.42 ms) ($n = 34$ cells, 271 trials).

Scale bars, 10 μ m. See also Table S1.

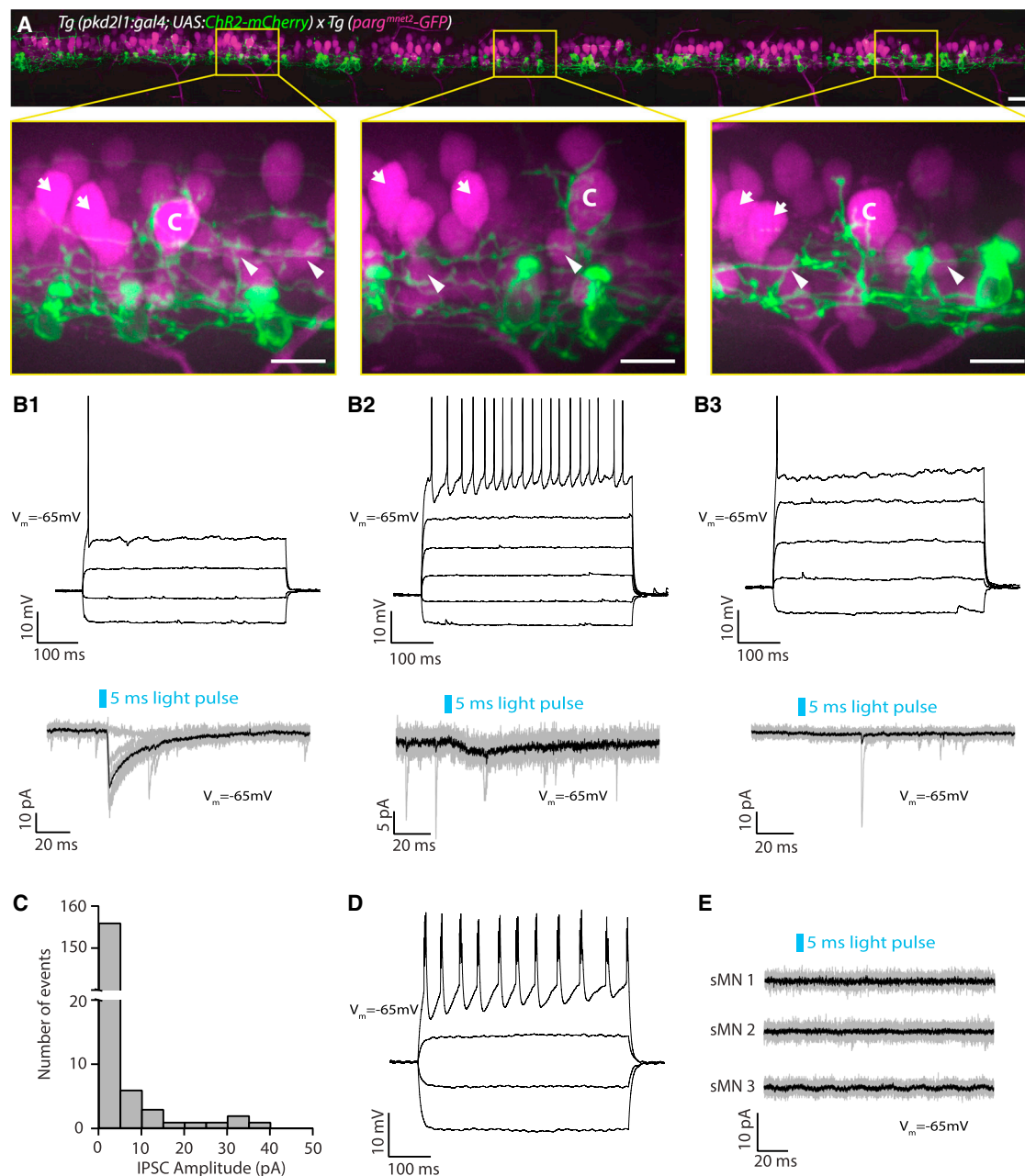


Figure 2. Motor Neurons Other Than CaPs Receive Limited CSF-cN Input

(A) Motor neurons and CSF-cNs labeled in the *Tg(pkcd211:gal4; UAS:ChR2-mCherry) x Tg(parg^{met2}-GFP)* transgenic line throughout the rostro-caudal axis (12 axial segments) at 3 dpf. Boxes with magnified images highlight extensive innervation of large dorsal CaP motor neurons (labeled “C”). However, other (non-CaP) primary motor neurons (indicated by arrows) and secondary motor neurons (indicated by arrowheads) do not exhibit the same extensive perisomatic innervation. Scale bars, 20 μ m (top) and 10 μ m (magnified boxes, bottom).

(B1–B3) Examples of whole-cell recordings from non-CaP primary motor neurons showing three types of postsynaptic responses observed.

(B1) Top: current-clamp recording of a primary motor neuron showing a single action potential in response to current injection (steps of 40 pA from -50 pA to $+70$ pA). Bottom: voltage-clamp recording from the same primary motor neuron ($V_m = -65$ mV) showing evoked IPSCs following 5-ms light pulses (black trace is the average of ten trials shown in gray).

(B2) Top: current-clamp recording of a primary motor neuron showing tonic action potentials in response to current injection (steps of 40 pA from -50 pA to $+150$ pA). Bottom: voltage-clamp recording from the same primary motor neuron ($V_m = -65$ mV) showing small evoked IPSCs following 5-ms light pulses (black trace is the average of ten trials shown in gray).

(B3) Top: current-clamp recording of a primary motor neuron showing a single action potential in response to current injection (steps of 40 pA from -30 pA to $+130$ pA). Bottom: voltage-clamp recording from the same primary motor neuron ($V_m = -65$ mV) showing no IPSCs following 5-ms light pulses (black trace is the average of ten trials shown in gray).

(C) Histogram of IPSC current amplitudes from non-CaP primary motor neurons (mean 1.78 ± 0.42 pA; $n = 17$ cells, 170 trials).

(legend continued on next page)

transgenic fish (Figure 2A). As shown previously, CaP motor neurons were distinguished based on soma location within the segment and the characteristic basket-like synaptic contacts from CSF-cNs (Figures 1A, 1B, 1E, and 2A; CaP motor neurons are indicated by “C” in magnified images). Responses for non-CaP primary motor neurons (Figure 2A, magnified boxes, indicated by arrows) following ChR2-mediated activation of CSF-cNs fell into three classes (Figures 2B). Only one non-CaP primary motor neuron out of 17 recorded showed IPSCs comparable to responses observed in CaP motor neuron recordings (Figure 2B1, lower panel). In 11 of 17 non-CaP primary motor neurons the postsynaptic responses were very small (<5 pA; Figure 2B2, lower panel), and in the remaining five non-CaP primary motor neurons no IPSCs were observed (Figure 2B3; lower panel). The majority of IPSCs observed in non-CaP primary motor neurons were of small amplitude (<5 pA; Figure 2C). All but two of the events greater than 10 pA were observed in trials from a single neuron (Figure 2B1), suggesting that CSF-cN innervation of primary motor neurons is preferentially targeted to CaP motor neurons. Secondary motor neurons were also tested for CSF-cN connectivity and were targeted based on fluorescence, ventral location, and small soma size in the *Tg(parg^{mn2}-GFP)* transgenic line (Figure 2A, magnified boxes, indicated by arrowheads). Secondary motor neurons showed typical bursting action potential firing patterns (see the example in Figure 2D); however, CSF-cN activation with 5-ms blue light pulses never produced IPSCs in secondary motor neurons in ten out of ten cells recorded (Figure 2E; three secondary motor neuron examples are shown). CSF-cNs therefore form very specific contacts within the motor pool to CaP motor neurons.

Optogenetic-Mediated Mapping Reveals Connectivity to Sensory Interneurons

We noted that some of the CSF-cN axons project to the dorsal spinal cord, suggesting that they target other spinal neurons. We hypothesized that they might target sensory interneurons in this population, and tested a subtype of glutamatergic interneuron (called commissural primary ascending interneuron [CoPA]) known to be involved in sensory-motor gating and recruitment of motor neurons in the contralateral spinal cord [19, 20]. By selectively labeling CoPA interneurons in the *Tg(tbx16-GFP)* line [21], we observed that some CSF-cN varicosities were located on the CoPA soma (Figures 3A1 and 3A2) and axon initial segment (Figures 3A1–3A4). Interestingly, we noted that the morphology of CSF-cN axons suggests that an individual CSF-cN in contact with CaP (forming the basket-like synapse) may also diverge onto the adjacent CoPA dendrite (Figures 3A3 and 3A4). We performed targeted whole-cell patch-clamp recordings (Figure 3B) and simultaneous photostimulation of CSF-cNs and found evidence of monosynaptic connections to CoPA interneurons (Figure 3C). CoPA IPSCs were large and did not fail (eight out of eight cells; Figure 3C). The IPSCs recorded in CoPA showed properties typical of GABA_A-mediated currents,

similar to the IPSCs recorded in CaP motor neurons (Figures 3D–3G). However, IPSC amplitudes tended to be larger for CoPA sensory interneurons than for those observed in CaP motor neurons (Figure 3H).

Convergence of Inputs from Multiple CSF-cNs onto Individual Targets

We took advantage of a 2D light-patterning approach [3, 22] to activate specific ChR2-expressing cells within the zebrafish spinal cord in order to test the connectivity of individual CSF-cNs to CaP and CoPA targets (Figure 4). We used a custom-built illumination setup based on a digital mirror device (Figure 4A) to pattern the stimulation light to spatially restricted targets (Figures 4B and 4C). The light stimulation was effective in triggering an IPSC only when it was directed onto the soma or occasionally onto the initial segment of CSF-cNs (Figure 4D), but not onto the rest of the axonal projection, including the varicosities within the basket structure surrounding the soma of the recorded cell (Figure 4D). The amplitude of IPSCs tended to decrease as a function of distance between the presynaptic CSF-cN and its target, with connections emanating from CSF-cNs less than three segments away from the target producing the largest responses (Figure 4E). Our data also show that multiple CSF-cNs often innervate the same target neuron, either the CaP motor neuron (Figures 4D, 4F, and 4G) or the CoPA interneuron (Figure 4H), indicating a high degree of convergence from CSF-cNs onto their targets.

Neither Commissural Glycinergic Neurons nor Mechanosensory Neurons Involved in the Escape Circuit Receive Inputs from CSF-cNs

We next sought to address whether the functional connectivity of CSF-cNs was specific to the glutamatergic interneurons and motor neurons of the escape circuit or whether they exert a distributed modulation impacting all elements of the escape pathway. We tested whether CSF-cNs project onto the contralaterally projecting glycinergic neurons, referred to as commissural local interneuron (CoLo) cells, involved in silencing activity on the contralateral side during the initial tail bends of the escape response [15] (Figures 5A–5C). Targeted patch-clamp recordings of CoLos using the *Tg(Tol-056-GFP)* transgenic line [15] (Figure 5A) showed no light-induced IPSCs in 13 out of 13 CoLos recorded (Figures 5B and 5C; three examples are shown). We also tested the connectivity to mechanosensory Rohon-Beard neurons that are well upstream of the escape circuit. Anatomical analysis of Rohon-Beard neurons and CSF-cNs in the *Tg(p2rx3.2:GFP; pkd211:gal4; UAS:ChR2-mCherry)* triple transgenic larvae showed no overlap of CSF-cN axons onto the Rohon-Beard somas or axons [23] (Figure 5D). Whole-cell recordings of Rohon-Beard neurons were performed to rule out functional connectivity to CSF-cNs (Figures 5E and 5F). IPSCs in Rohon-Beard neurons were never observed following ChR2-mediated activation of CSF-cNs with 5-ms light pulses

(D) Current-clamp recording of a secondary motor neuron showing bursts of action potentials in response to current injection (steps of 20 pA from –30 pA to +30 pA).

(E) Example of voltage-clamp recordings from secondary motor neurons (SMNs) ($V_m = -65$ mV) showing no IPSCs following 5-ms light pulses (black trace is the average of ten trials shown in gray). IPSCs in secondary motor neurons were never observed following CSF-cN stimulation ($n = 10$).

See also Table S1.

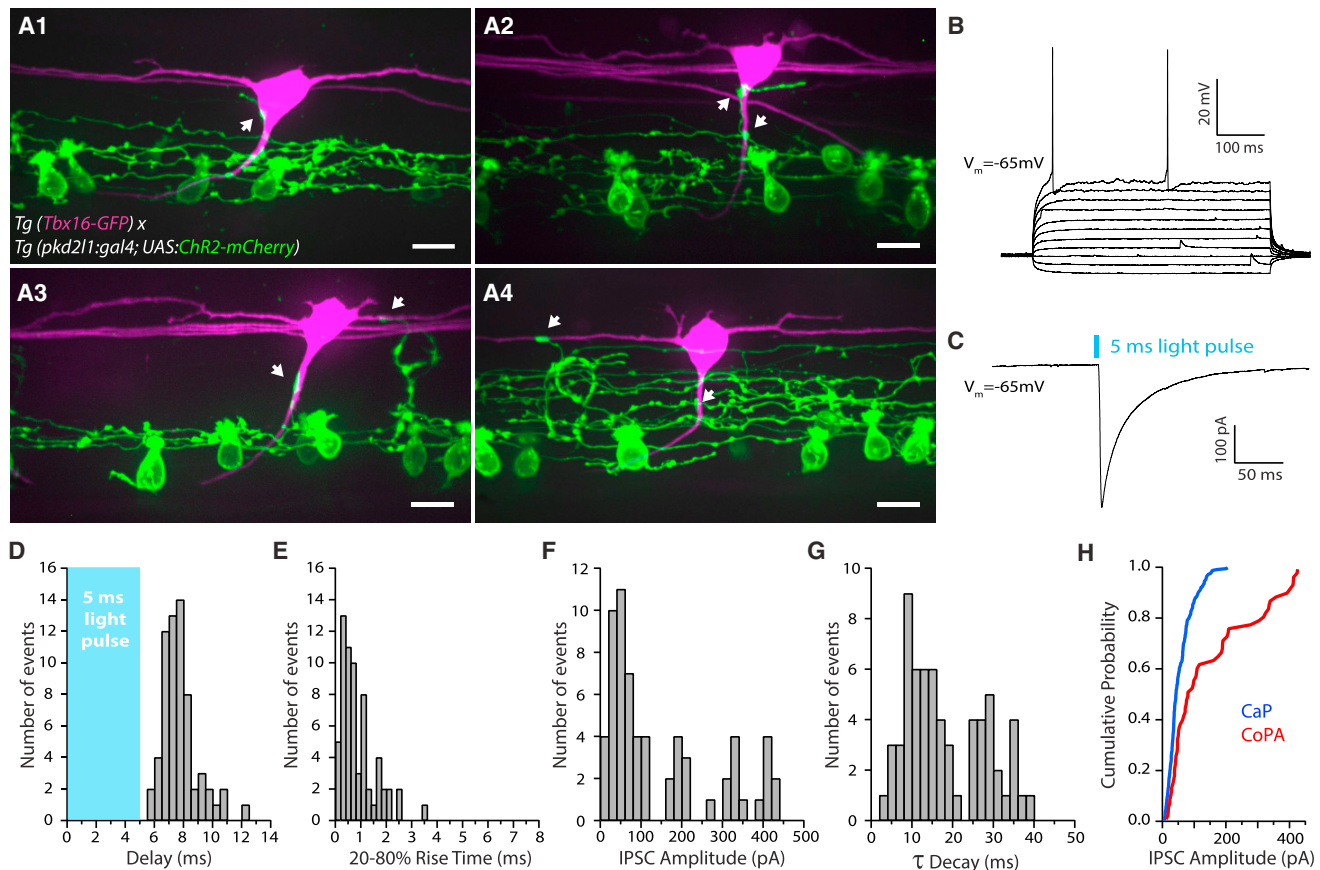


Figure 3. CSF-cNs Innervate CoPA Glutamatergic Sensory Interneurons

(A1–A4) Z projection stack showing CoPA sensory interneurons expressing GFP (magenta) innervated by CSF-cNs (green) in *Tg(pkcd211:gal4; UAS:ChR2-mCherry; tbx16:GFP)* transgenic larvae. Note the varicosities (arrows) from CSF-cNs onto CoPA soma (A1 and A2), initial segment (A2 and A3), and sometimes dendrites (A3 and A4). Scale bars, 10 μ m.

(B) Current-clamp recording of a typical CoPA interneuron showing sparse action potential firing in response to current injections (steps are 20 pA from -50 pA to $+150$ pA).

(C) Voltage-clamp recording from a CoPA interneuron ($V_m = -65$ mV) showing an evoked IPSC following a 5-ms light pulse (black trace; average of ten trials).

(D–G) Distribution of IPSC delay (D; mean 7.73 ± 0.15 ms), 20%–80% rise time (E; mean 0.88 ± 0.08 ms), amplitude (F; mean 146.83 ± 16.75 pA, corresponding to a conductance of 10.49 nS), and time decay τ (G; mean 18.16 ± 1.22 ms) ($n = 8$ cells, 64 trials).

(H) Cumulative probability plot of IPSC amplitudes for CaP motor neurons (blue; $n = 271$) and CoPA interneurons (red; $n = 64$).

See also Table S1.

(Figure 5F; $n = 10$; three examples are shown). Taken together, our data establish a map of CSF-cN innervation onto specific elements of the escape circuit. CSF-cNs create extensive synaptic contacts specifically to CaP motor neurons and CoPA glutamatergic sensory interneurons with minimal projections onto other primary motor neurons, and an exclusion of projections onto secondary motor neurons, CoLo glycinergic commissural interneurons, and Rohon-Beard mechanosensory neurons.

CSF-cN Synapses onto Targets of the Escape Circuit Show Strong Short-Term Depression

Common features of CSF-cN-mediated IPSCs recorded from CaP motor neurons and sensory interneurons include their high reliability and large amplitude (Figures 6A1–6A3). Because CSF-cNs are recruited by spinal curvature during active locomotion [7], we tested whether these synapses showed short-term plasticity when stimulated at higher frequencies corresponding

to larval swimming (10–20 Hz; Figures 6C and 6D). Whereas 1-Hz stimulation induced moderate short-term depression following ten light pulses (Figures 6B1–6B3), raising the stimulation frequency to 10 and 20 Hz led to an incremental increase in short-term synaptic depression (Figures 6C1–6C3 and 6D1–6D3).

A Single CSF-cN Action Potential Leads to Prompt Silencing of Spiking in CSF-cN Targets within the Escape Circuit

Although we showed that CSF-cN firing causes a large and reliable chloride conductance in CaP motor neurons and CoPA sensory interneurons, the impact of this modulation on the output of the CPG, namely motor neuron activity, was unclear. It has been suggested that an immature chloride gradient in the larval spinal cord could lead GABAergic input to be depolarizing in postsynaptic neurons [24]. We therefore tested how CSF-cNs modulated the spiking of their motor neuron targets by recording CaP motor

neurons in cell-attached mode to preserve the chloride gradient in the postsynaptic neuron. A large voltage step induced high-frequency firing in CaP motor neurons in this configuration (Figures 7A and 7B). A 5-ms light pulse (producing a single large IPSC) was sufficient to transiently silence the spiking of CaP motor neurons (Figures 7B and 7C). Quantification of the maximum interspike interval (ISI) for control trials and trials where a 5-ms light pulse activated CSF-cNs showed a significant increase after the light pulse in all cells tested (ISI control, 9.10 ± 3.04 ms; ISI light, 26.69 ± 10.55 ms; $n = 4$), confirming the inhibitory nature of the GABAergic IPSCs from CSF-cNs onto their targets (Figure 7D).

CSF-cNs Are Mechanosensory Cells that Control Balance during Fast Locomotion

We monitored CSF-cN activity using the genetically encoded calcium indicator GCaMP3 combined with the position marker mCherry in unparalyzed larvae, which were mounted on their side and embedded in agarose. In these conditions, we found that ventral CSF-cNs are recruited during spontaneous longitudinal contractions (Figure S1; Movie S1). Imaging and functional mapping experiments suggest that only ventral CSF-cNs, not dorsal CSF-cNs, innervate CaP motor neurons involved in postural control (Figures 1E, 4D, 4F, and 4G). From these results, we hypothesized that ventral CSF-cNs could act as a mechanosensory system detecting longitudinal spinal bending and subsequently provide inhibitory tone to CaP motor neurons. We tested this hypothesis by analyzing the behavior of animals in which CSF-cN synapses were silenced by botulinum toxin [7]. We reanalyzed the dataset from Böhm et al. [7], and rollover events were scored by a blinded observer. We determined a roll ratio for each fish (number of trials the fish rolled/number of trials the fish responded to the acoustic stimulus) and found that rollovers occurred twice as often in animals expressing botulinum toxin in CSF-cNs compared to control siblings (Figures 7E and 7F; Movies S2 and S3). This result indicates that CSF-cNs contribute to maintaining balance during active locomotion.

DISCUSSION

Selective Inhibition from GABAergic Sensory Neurons to Sensory Interneurons and Motor Neurons of the Escape Circuit

Our work demonstrates a strong and selective connection from CSF-cNs to primary motor neurons and glutamatergic sensory interneurons (CaP and CoPA, respectively). This connectivity appears to be specific within the escape circuit of the zebrafish spinal cord, as CSF-cNs avoid synaptic contacts to secondary motor neurons, mechanosensory neurons, and glycinergic premotor interneurons, which are involved in escapes. CSF-cN input to motor neurons is mainly limited to the primary motor neuron, CaP, whereas other primary motor neurons generally receive little to no synaptic input. The specificity of the CSF-cN synapse onto CaP motor neurons suggests that these motor neurons may play a specialized role that differs from other primary motor neurons. CaP motor neurons are the first motor neurons to extend from the spinal cord to the skeletal muscle in the developing embryo [18]. Primary motor neurons (CaPs, middle primary motor neurons [MiPs], and the two rostral primary motor

neurons [RoPs]) innervate distinct territories of axial, fast skeletal muscle fibers. Of the primary motor neurons, CaP innervates the largest field of fast skeletal muscle, covering approximately two-thirds of the ventral fibers. The differential activation of primary motor neurons is thought to induce body torque and therefore a change in vertical trajectory [16]. Beyond their importance in fast locomotion and the escape response, CaP motor neurons most likely play a role in maintaining postural control. In this study, we observe that CSF-cNs project selectively onto CaP motor neurons, and that the silencing of CSF-cNs leads to a balance defect causing larvae to tip and roll over during acoustically induced escape responses. This observation suggests that inhibition to CaP motor neurons by CSF-cNs plays a critical role in the control of posture during fast swimming. However, we cannot exclude that other putative targets of CSF-cNs contribute to this effect as well.

Physiology of CSF-cN Synapses onto Their Targets within the Escape Circuit

The somatic and axonic innervation of CSF-cNs onto CaP motor neurons and CoPA interneurons is enhanced by the convergence of inputs from multiple CSF-cNs onto one target neuron. This convergence is reminiscent of the projection from basket cells onto pyramidal neurons [25–28], and is associated with large reliable IPSCs. The CSF-cN-mediated inhibition from a single spike is efficient enough to transiently silence postsynaptic targets within the escape circuit. At higher stimulation frequencies, synapses of CSF-cNs onto their targets rapidly depress. In direct recordings from CSF-cNs in the cell-attached configuration, optogenetically mediated activation of CSF-cNs has been confirmed up to 25 Hz without action potential failures. We therefore believe that the observed plasticity most likely reflects a presynaptic mechanism consistent with other high release probability synapses that undergo short-term depression rather than failure to optogenetically elicit spiking in CSF-cNs. Remarkably, the short-term depression occurs at frequencies that closely match the naturally occurring tail beat frequencies of zebrafish larvae. A result of this property is that within this range of CSF-cN firing frequencies, the first IPSC is the most effective at modulating the spiking of motor and sensory interneuron targets. This feature suggests a homeostatic function for the feedback inhibition provided by CSF-cNs: large motor neurons triggering the massive muscle contractions during the C-bend also recruit GABAergic sensory neurons that rapidly silence them.

The physiology of CSF-cN synapses onto elements of the fast escape circuit shown here is remarkably different from their modulation of the slow swimming circuit [5]. The connections from CSF-cNs to multipolar commissural descending interneuron [MCoD], which are glutamatergic premotor interneurons, produce small-amplitude IPSCs that are subject to failures and facilitate during repetitive stimulation [5]. In contrast, the projections of CSF-cNs onto both CaP and CoPA targets within the escape circuit are large, show no failure, and rapidly depress over time. During repetitive contractions when the animal swims at high speed, this GABAergic sensory-motor pathway may therefore promptly silence motor neurons and interneurons involved in the initial phase of the escape, enabling a tight control of spike timing of motor neurons and a rapid transition from fast to slow swimming frequencies [29].

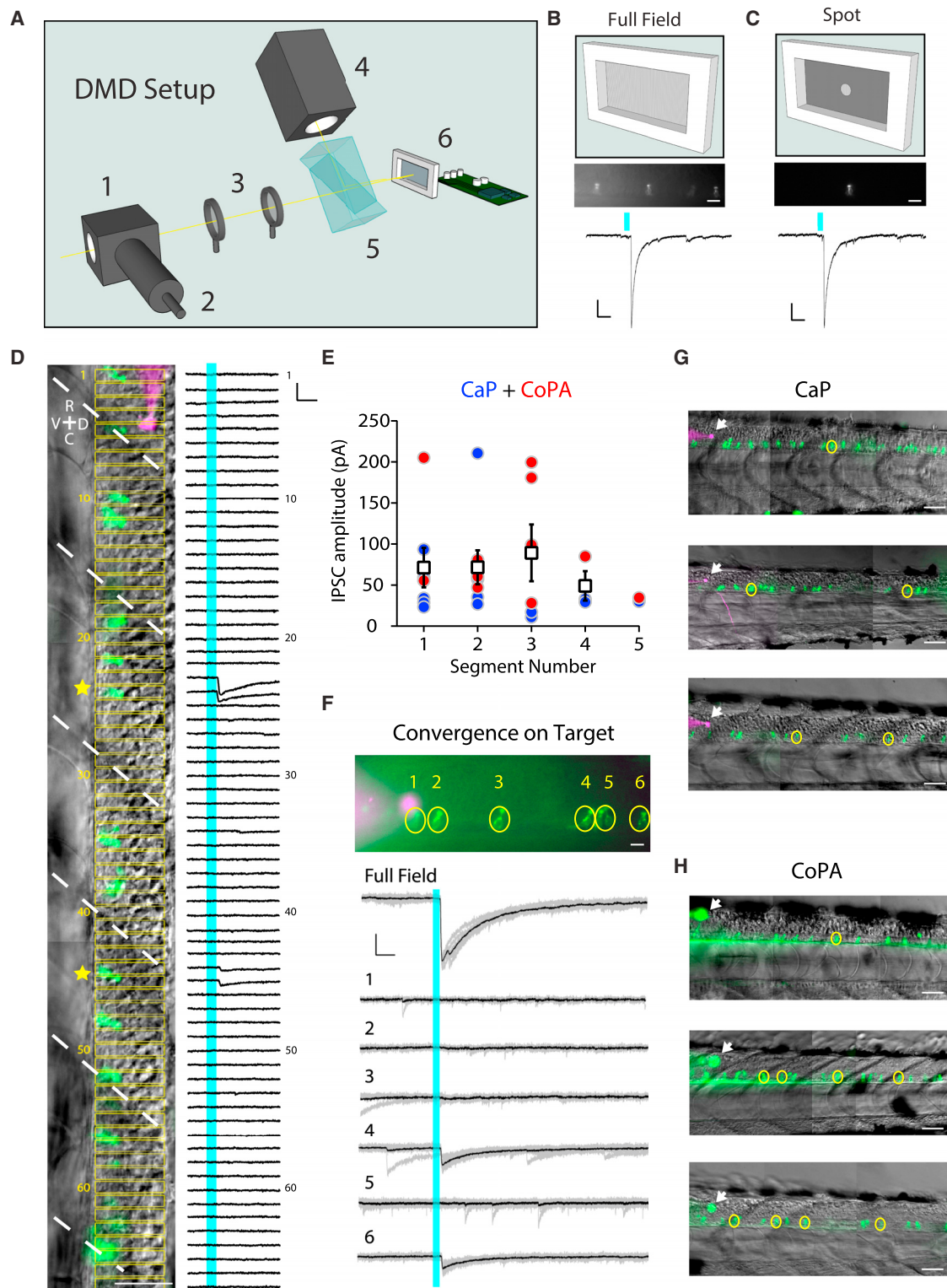


Figure 4. 2D Light Patterning at Single-Cell Resolution Reveals Convergence of Inputs from CSF-cNs onto Their Targets

(A) Schematic of the digital mirror device (DMD) setup showing the light path. A beamsplitter (1) was attached to the epi-port of an upright microscope in order to combine light from the epifluorescence light source via an optical fiber (2) and the light from the DMD. The patterned light from the DMD was relayed into the epifluorescence light path via a telescope (3). A white light-emitting diode (LED) (4) providing the light for patterned illumination was directed via a total internal reflection prism (5) to the DMD (6).

(legend continued on next page)

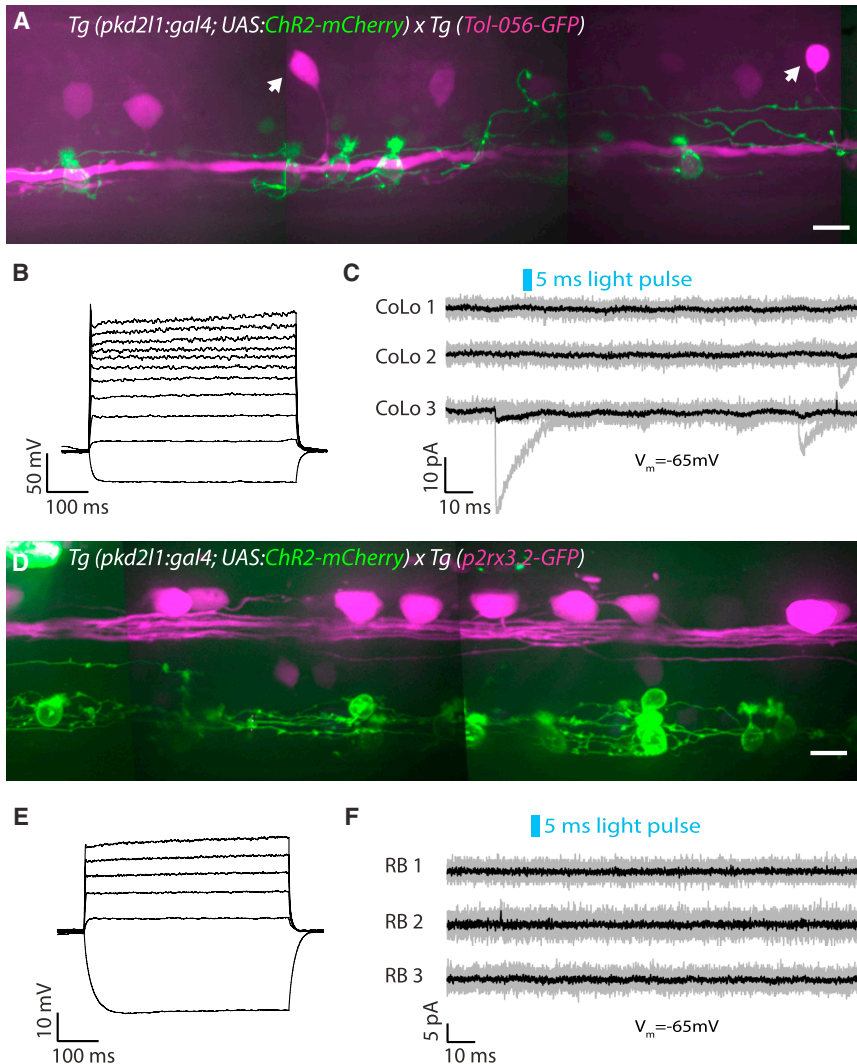


Figure 5. CSF-cN Local Innervation onto the Escape Circuit Is Restricted to Excitatory Interneurons and Motor Neurons

(A) Z projection stack of CoLo glycinergic premotor interneurons expressing GFP (magenta) and CSF-cNs (green) in a *Tg(pkd2l1:gal4; UAS:ChR2-mCherry; Tol-056-GFP)* transgenic larva at 3 dpf. Arrows indicate CoLo cell bodies. Scale bar, 10 μ m.

(B) Current-clamp recording showing the typical firing pattern of a CoLo neuron with a single weak action potential in response to current injection (steps of 20 pA from -30 pA to $+370$ pA).

(C) CSF-cN stimulation elicited by a 5-ms light pulse fails to induce an IPSC in CoLos. Example of voltage-clamp recordings from three CoLos ($V_m = -65$ mV) showing no IPSCs following 5-ms light pulses (black trace is the average of ten trials shown in gray). IPSCs in CoLos were never observed following CSF-cN stimulation ($n = 13$ cells).

(D) Z projection stack showing Rohon-Beard neurons expressing GFP (magenta) and CSF-cNs (green) in a *Tg(pkd2l1:gal4; UAS:ChR2-mCherry; p2rx3.2:GFP)* transgenic larva at 3 dpf. Note that the axonal projections of CSF-cNs do not reach Rohon-Beard somas or axons. Scale bar, 10 μ m.

(E) Current-clamp recording showing the typical firing pattern of a Rohon-Beard neuron with a single weak action potential in response to current injection (steps of 20 pA from -30 pA to $+170$ pA).

(F) CSF-cN stimulation elicited by a 5-ms light pulse fails to induce an IPSC in Rohon-Beard (RB) neurons. Example of voltage-clamp recordings from three Rohon-Beard neurons ($V_m = -65$ mV) showing no IPSCs following 5-ms light pulses (black trace is the average of ten trials shown in gray). IPSCs in Rohon-Beard neurons were never observed following CSF-cN stimulation ($n = 10$ cells).

See also [Table S1](#).

Relevance to Physiology and Postural Control

As indicated by anatomy [3, 5, 30–33], we demonstrate, using physiology and optogenetics, that the GABAergic sensory feedback provided on the escape circuit is local and intraspinal, never reaching targets more than five segments away in the larval stage.

This GABAergic pathway can therefore locally tune the excitability of components of the escape in the spinal cord, without affecting the activity of reticulospinal neurons in the hindbrain.

Fast escapes in zebrafish larvae are highly regulated in terms of both lateral displacement and vertical elevation [34], so that

(B and C) Physiological responses to either full-field illumination (B) or a small spot on an individual CSF-cN (C). Top: fluorescent image of multiple CSF-cNs from the *Tg(pkd2l1:gal4; UAS:ChR2-mCherry)* transgenic line with all (B) or a subset of the central mirrors activated (C). Scale bars, 20 μ m. Bottom: IPSCs following a 5-ms light pulse from either full-field (B) or patterned illumination (C). In cases where only one CSF-cN is connected to the target, the IPSC amplitude evoked by the spot recapitulates the IPSC amplitude evoked by the full-field illumination. Scale bars, 50 ms horizontal and 20 pA vertical.

(D) Example experiment investigating the connectivity from CSF-cNs (green) to a CaP motor neuron (magenta) showing multiple CSF-cNs projecting onto the postsynaptic target. Light was patterned in rectangles (indicated in yellow), which were sequentially illuminated along the rostro-caudal axis during voltage-clamp recording of the target neuron. Right: voltage-clamp traces resulting from the light activation of the corresponding rectangular region. IPSCs are observed when the light is patterned onto a subset of CSF-cNs (yellow stars). White dashed lines indicate segment boundaries. Scale bars, 50 μ m (image) and 10 ms horizontal and 50 pA vertical (electrophysiological traces).

(E) Quantification of the IPSC amplitude for CaP (blue circles) and CoPA (red circles) as a function of the number of segments between a CSF-cN and its target. Mean IPSC amplitude for CaP and CoPA combined is plotted for each segment (white boxes).

(F) Convergence of CSF-cNs onto a CaP motor neuron. Image of CSF-cNs expressing ChR2-mCherry (green) and the target CaP motor neuron filled with Alexa dye (magenta). IPSCs in response to either full-field or patterned illumination show that cells “4” and “6” converge onto the CaP motor neuron target.

(G and H) Examples of identified connections from CSF-cNs to CaP motor neurons (G) and CoPA neurons (H) in three different larvae. Arrows indicate the patched target cell body. Yellow circles show connected CSF-cNs. Scale bars, 50 μ m.

See also [Table S1](#).

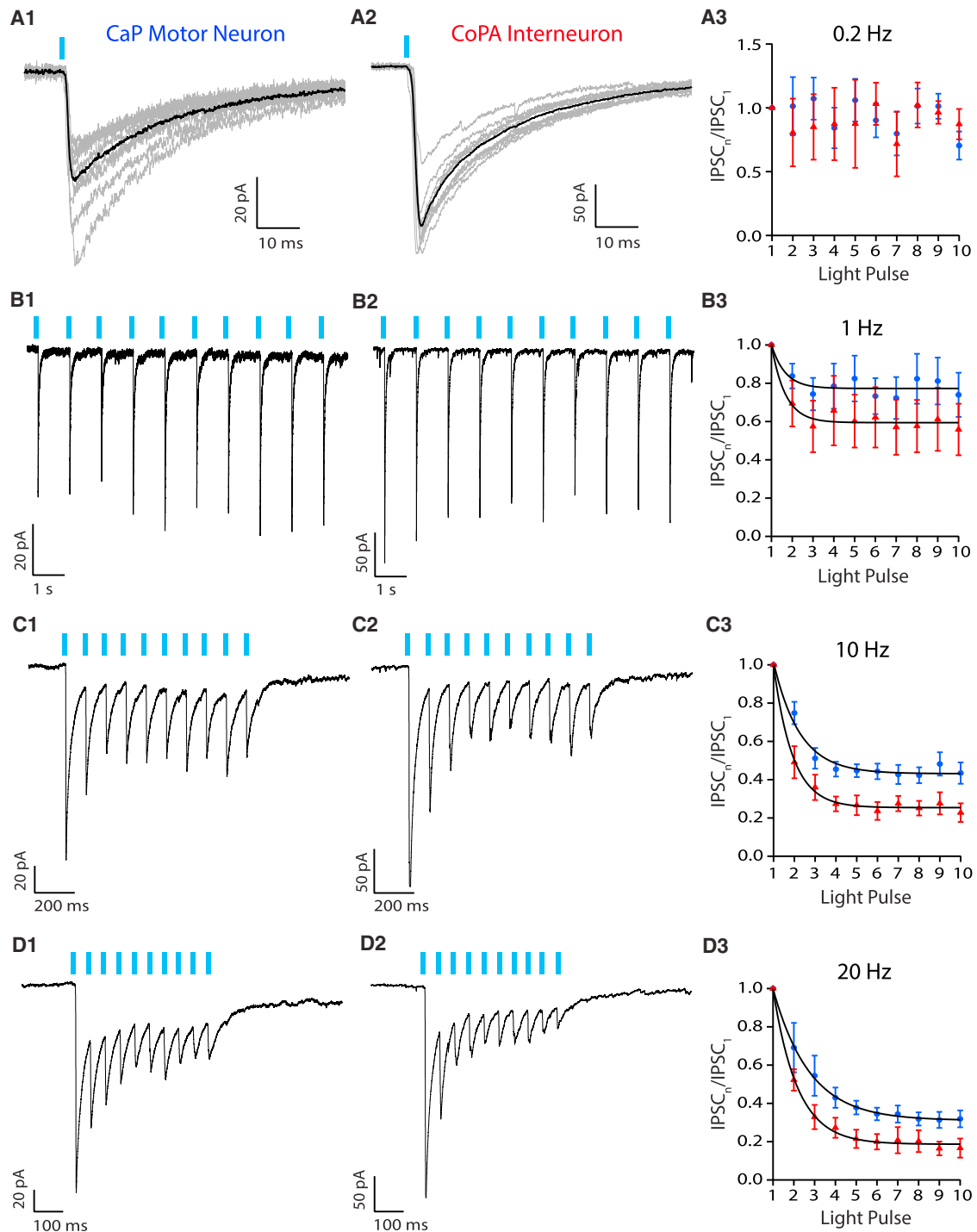


Figure 6. Stimulation of CSF-cNs at Moderate Frequencies Results in Short-Term Synaptic Depression in CaP Motor Neurons and CoPA Interneurons

(A1 and A2) Typical examples of IPSCs (gray) recorded from CaP (A1) and CoPA (A2) at 0.2 Hz. The average of ten trials is in black. Note the absence of failure and the large IPSC amplitude.

(A3) Stimulation at 0.2 Hz induced moderate short-term depression in CaP (blue circles; t test for the difference between the first and tenth light pulse; $p = 0.036$, $n = 7$) and no depression for CoPA (red triangles; $p = 0.48$, $n = 5$).

(B1 and B2) Typical examples of IPSCs recorded from CaP (B1) and CoPA (B2) at 1 Hz. The trace is an average of ten trials. Note the absence of failure of the IPSC.

(B3) Trains of stimuli at 1 Hz induce small but significant short-term depression (23% for CaP, blue circles, $p = 0.037$, $n = 7$; 41% for CoPA, red triangles, $p = 0.030$, $n = 5$).

(legend continued on next page)

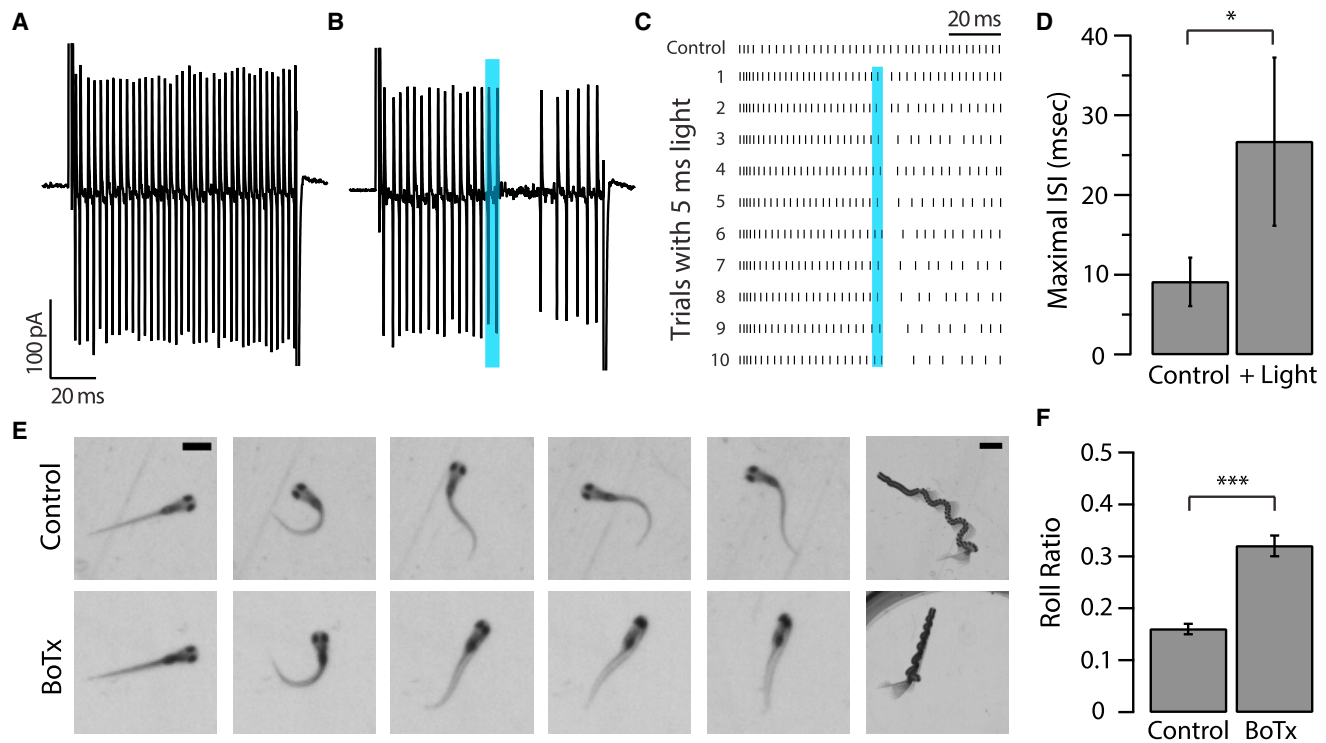


Figure 7. Silencing CSF-cNs Induces a Defect in Balance during Fast Swimming

(A) A voltage step (+180 mV for 100 ms from a holding potential of -65 mV) in cell-attached mode leads to high-frequency CaP motor neuron spiking in the control condition.

(B) Typical trial showing that in a *Tg(pkcd211:gal4; UAS:ChR2-mCherry)* transgenic larva a 5-ms light pulse applied during the voltage step leads to the prompt silencing of the CaP motor neuron for approximately 20 ms.

(C) Raster plot of CaP spiking without (top trace) and with (bottom ten traces) optogenetic stimulation of CSF-cNs. Repetition of ten sequential trials confirmed the robust effect of silencing CaP firing. The duration of silencing tended to increase during sequential trials.

(D) Maximum interspike interval (ISI) was quantified for five spikes prior to the light pulse and five spikes following the light pulse. All cells showed silencing following the 5-ms light pulse, illustrated by an increase in ISI (9.10 ms \pm 3.04 ms before and 26.69 ms \pm 10.55 ms after the light pulse; $n = 4$, paired t test: $*p = 0.02$).

(E) Sample sequence of images acquired with a high-speed camera during acoustically evoked escaped responses for *Tg(pkcd211:gal4; UAS:BoTxBLC-GFP)* transgenic larvae and control siblings. Magnified images (five panels on the left) demonstrate the rolling phenotype when CSF-cNs are genetically targeted with *BoTxBLC-GFP*⁺ to silence GABA release (scale bars, 1 mm). Z stack of the entire escape response sequence for *BoTxBLC-GFP*⁺ and control siblings (panels on the right; scale bars, 2 mm).

(F) Calculated roll ratio for *Tg(pkcd211:gal4; UAS:BoTxBLC-GFP)* transgenic larvae and control siblings ($n = 148$ fish for each genotype). *BoTxBLC-GFP*⁺ fish were significantly more likely to tip over and roll during the escape response than the control siblings ($***p < 0.001$).

See also [Figure S1](#), [Table S1](#), and [Movies S1](#), [S2](#), and [S3](#).

larvae do not perform spiral trajectories as seen in *Xenopus* tadpoles [35]. Control of posture most certainly involves visual and vestibular feedback relayed by reticulospinal neurons down the spinal cord in order to optimally activate primary motor neurons [36]. Here we describe a local sensory-motor pathway for regulating posture situated within the spinal cord, a concept that to our knowledge has only been described in birds, where balance is stabilized by the vestibular organ during flight and by the

lumbosacral system during walking [37]. By genetically targeting the optimized botulinum toxin to selectively block synaptic release from CSF-cNs, we observed a balance defect in botulinum toxin (BoTx) fish compared to control siblings not expressing the toxin. Animals with CSF-cN neurotransmission silenced were twice as likely as their wild-type siblings to tip and roll over during an acoustically induced escape response. In addition, we show that ventral CSF-cNs project onto CaP motor

(C1 and C2) Typical examples of IPSCs recorded from CaP (C1) and CoPA (C2) at 10 Hz. The trace is an average of ten trials. Note the absence of failure and the promptly decreasing amplitude of the IPSC.

(C3) Trains of stimuli at 10 Hz induce large, significant short-term depression (57% for CaP, blue circles, $p = 0.00002$, $n = 7$; 75% for CoPA, red triangles, $p = 0.00009$, $n = 5$).

(D1 and D2) Typical examples of IPSCs recorded from CaP (D1) and CoPA (D2) at 20 Hz. The trace is an average of ten trials. Note the absence of failure and the promptly decreasing amplitude of the IPSC.

(D3) Trains of stimuli at 20 Hz induce large, significant short-term depression (68% for CaP, blue circles, $p = 0.000008$, $n = 7$; 81% for CoPA, red triangles, $p = 0.00005$, $n = 5$).

neurons and are physiologically activated during longitudinal contractions, which is not the case in differential left or right bending of the tail [7]. These results point to an asymmetrical proprioceptive function for CSF-cNs, whereby dorsal CSF-cNs respond to left or right horizontal bending, whereas ventral CSF-cNs respond to longitudinal bending of the spinal cord. CSF-cNs would therefore provide mechanosensory feedback during locomotion to inhibit motor output through the specific connectivity to the CaP motor neuron and excitatory interneurons such as CoPAs and MCoDs. CSF-cNs therefore may constitute a mechanosensory system within the spinal cord that provides important proprioceptive feedback to coordinate locomotion and balance. The CSF-cNs may themselves be modulated by reticulospinal neurons or vestibulospinal pathways involved in the control of posture. This will be the focus of future investigations, as descending inputs were severed by decapitation prior to testing intraspinal CSF-cN connectivity in this study.

EXPERIMENTAL PROCEDURES

Animal Care and Transgenics Used

Animal handling and procedures were validated by the Institut du Cerveau et de la Moelle épinière (ICM) and the French National Ethics Committee (Comité National de Réflexion Éthique sur l'Expérimentation Animale; Ce5/2011/056) in agreement with European Union legislation. Adults were reared at a maximal density of eight animals/L in a 14/10-hr (light/dark) cycle environment. Fish were fed live artemia twice a day, and the feeding regime was supplemented with solid extracts matching the developmental stage (ZM Systems). Larvae were raised at 28.5°C with a 14/10-hr (light/dark) light cycle. Experiments were performed at room temperature (22°C–25°C) on 3- to 7-dpf (days post-fertilization) larvae. All transgenic lines used here are detailed in Table S1. We injected the *UAS:synaptophysin-GFP* [38] DNA construct at 60 ng/μL into *Tg(pkd21:gal4; UAS:ChR2-mCherry)* single-cell-stage embryos.

Electrophysiology

3- to 7-dpf zebrafish larvae were decapitated and pinned to a Sylgard-coated recording chamber (Sylgard 184; Dow Corning) through the notochord with electrolytically sharpened tungsten pins. The skin was removed and the specimen was bathed briefly in a 10% formamide solution and subsequently washed in bath recording solution to eliminate spontaneous muscle twitching. The dura was exposed by suctioning away dorsal muscle fibers with a glass pipette. Typically, three to seven segments of dorsal muscle were removed. Recording electrodes were fashioned from capillary glass (1.5 mm outer diameter [O.D.], 1.1 mm inner diameter [I.D.]; WPI) with a horizontal puller (P1000; Sutter Instrument). Electrode resistances were 10–16 MΩ. Positive pressure (65 mm Hg) was applied to the recording electrode via a pneumatic transducer (Fluke Biomedical; DPM1B). Once the electrode was driven through the dura in order to approach neurons targeted for patch experiments, the positive pressure was reduced to 35 mm Hg [39]. Cells were chosen based on their soma location matching the axonal projections of CSF-cNs expressing ChR2-mCherry and the expression of GFP in the transgenic lines used (Table S1). External bath recording solution contained the following: 134 mM NaCl, 2.9 mM KCl, 2.1 mM CaCl₂·H₂O, 1.2 mM MgCl₂, 10 mM glucose, and 10 mM HEPES, with the pH adjusted to 7.4 and osmolarity to 290 mOsm. Spinal neuron internal solution contained the following: 115 mM K-gluconate, 15 mM KCl, 2 mM MgCl₂, 0.5 mM EGTA, 4 mM Mg-ATP, 10 mM HEPES (pH 7.2), and 290 mOsm. All reagents were obtained from Sigma-Aldrich unless otherwise noted. Patch electrodes contained 40 μM Alexa Fluor 488 or 594 hydrazide (Life Technologies). Physiological recordings were made with an Axopatch 700B amplifier and digitized with a Digidata 1440A (Molecular Devices). pClamp software was used to acquire electrophysiological data at a sampling rate of 50 kHz and low pass filtered at 2.2 kHz. Data were analyzed with Clampfit (Molecular Devices), Igor Pro 6.34 (WaveMetrics), Excel 2010 (Microsoft), and Matlab (MathWorks). Summary data are presented as average ± SEM.

Confocal Imaging

For imaging, larvae were prepared as described for physiological recordings. Confocal images were acquired with an Evolve 10 MHz digital monochrome EMCCD camera (Photometrics) using a Yokogawa X1 spinning disk mounted to an upright wide-field microscope (Axio Examiner Z1; Zeiss) equipped with 20×, 40×, and 63× water-dipping objectives. Laser lines used here were a 50 mW 488-nm laser for imaging GFP and a 50 mW 561 nm laser for imaging mCherry. Z stacks were taken at 0.5 μm step size. Data were acquired using SlideBook 6 image acquisition software (3i). Images were assembled with ImageJ (NIH) and Photoshop and Illustrator CS6 (Adobe Systems).

2D Light Patterning Using a Digital Mirror Device

To generate the patterned illumination, we used a DLP Discovery kit (Texas Instruments) including a 0.7" digital mirror device (DMD) and API software (ViALUX). The DMD was imaged via a telescope (f 80 and 40 mm; Thorlabs) onto the back focal plane of the epifluorescence light path of an upright wide-field microscope (Axio Examiner D1; Zeiss). The DMD light path was combined with the epifluorescence light source via a 30% reflection, 70% transmission beamsplitter (AHF) to allow the patterned and epifluorescence illumination through the same path. As a light source for the patterned illumination, we used an ultra-high-power white LED (Prizmatix). The LED was coupled to the light path of the DMD via a total internal reflection prism (Lida Optical and Electronic). For fluorescence imaging and target cell selection, the microscope was equipped with an EMCCD camera (ImageEM; Hamamatsu). Integrated software control of the DMD and the camera was done via custom scripts in LabVIEW (National Instruments) and Matlab (MathWorks). The Matlab code was partly based on Zhu et al. [40].

Behavior Setup and Analysis

The behavior setup was previously described [7]. Each larva was subjected to five trials, and rolling behavior was assessed for each trial. The roll ratio was calculated as the number of trials the animal rolled during an escape divided by the number of trials the animal attempted an escape. Roll ratios for botulinum toxin light chain B (BoTxBLC)-GFP* fish and control siblings are presented as average ± SEM. Larvae were screened for GFP fluorescence to establish BoTx-positive and BoTx-negative siblings prior to data acquisition, and the experimenter was blinded to genotype prior to assessment of the rolling behavior.

SUPPLEMENTAL INFORMATION

Supplemental Information includes Supplemental Experimental Procedures, one figure, one table, and three movies and can be found with this article online at <http://dx.doi.org/10.1016/j.cub.2016.08.026>.

AUTHOR CONTRIBUTIONS

Conceptualization, J.M.H., C.S., and C.W.; Methodology, J.M.H., U.L.B., A.P., P.-E.B.T., C.S., and C.W.; Software, U.L.B.; Formal Analysis, J.M.H. and C.W.; Investigation, J.M.H.; Resources, M.N. and C.W.; Writing, J.M.H. and C.W., with input from all authors; Visualization, J.M.H.; Funding Acquisition, J.M.H., U.L.B., A.P., and C.W.; Supervision, C.W.

ACKNOWLEDGMENTS

We thank Prof. Shin-Ichi Higashijima, Prof. Dariusz Balciunas, Prof. David McLean, Prof. Mark Voigt, and Prof. Herwig Baier for kindly sharing transgenic lines. We thank Natalia Maties, Bodgan Buzurin, and Sophie Nunes Figueiredo from the ICM zebrafish facility for fish care. This work received support from the ICM, Ecole des Neurosciences de Paris, Fondation Bettencourt-Schueller, City of Paris Emergence program, Atip/Avenir program from the CNRS and INSERM, Marie Curie Actions (International Reintegration Grant; IRG 227200), ERC Starting Grant Optoloco (311673), Philippe Foundation, and Wings for Life Foundation (contract WFL-FR-009/14, project 91).

Received: June 29, 2016

Revised: August 8, 2016

Accepted: August 10, 2016

Published: October 6, 2016

REFERENCES

1. Kolmer, W. (1921). Das "Sagittalorgan" der Wirbeltiere. *Z. Anat. Entwicklungs* 60, 652–717.
2. Agduhr, E. (1922). Über ein Zentrales Sinnesorgan bei den Vertebraten. *Z. Anat. Entwicklungs* 66, 223–360.
3. Wyart, C., Del Bene, F., Warp, E., Scott, E.K., Trauner, D., Baier, H., and Isacoff, E.Y. (2009). Optogenetic dissection of a behavioural module in the vertebrate spinal cord. *Nature* 461, 407–410.
4. Orts-Del'Imagine, A., Wanaverbecq, N., Tardivel, C., Tillement, V., Dallaporta, M., and Trouslard, J. (2012). Properties of subependymal cerebrospinal fluid contacting neurones in the dorsal vagal complex of the mouse brainstem. *J. Physiol.* 590, 3719–3741.
5. Fidelin, K., Djenoune, L., Stokes, C., Prendergast, A., Gomez, J., Baradel, A., Del Bene, F., and Wyart, C. (2015). State-dependent modulation of locomotion by GABAergic spinal sensory neurons. *Curr. Biol.* 25, 3035–3047.
6. Jalalvand, E., Robertson, B., Wallén, P., and Grillner, S. (2016). Ciliated neurons lining the central canal sense both fluid movement and pH through ASIC3. *Nat. Commun.* 7, 10002.
7. Böhm, U.L., Prendergast, A., Djenoune, L., Nunes Figueiredo, S., Gomez, J., Stokes, C., Kaiser, S., Suster, M., Kawakami, K., Charpentier, M., et al. (2016). CSF-contacting neurons regulate locomotion by relaying mechanical stimuli to spinal circuits. *Nat. Commun.* 7, 10866.
8. Huang, A.L., Chen, X., Hoon, M.A., Chandrashekar, J., Guo, W., Tränkner, D., Ryba, N.J., and Zuker, C.S. (2006). The cells and logic for mammalian sour taste detection. *Nature* 442, 934–938.
9. Djenoune, L., Khabou, H., Joubert, F., Quan, F.B., Nunes Figueiredo, S., Bodineau, L., Del Bene, F., Burcklé, C., Tostivint, H., and Wyart, C. (2014). Investigation of spinal cerebrospinal fluid-contacting neurons expressing PKD2L1: evidence for a conserved system from fish to primates. *Front. Neuroanat.* 8, 26.
10. Jalalvand, E., Robertson, B., Tostivint, H., Wallén, P., and Grillner, S. (2016). The spinal cord has an intrinsic system for the control of pH. *Curr. Biol.* 26, 1346–1351.
11. Stoessel, M.E., Uhl-Bronner, S., Hugel, S., Veinante, P., Klein, M.J., Mutterer, J., Freund-Mercier, M.J., and Schlichter, R. (2003). Cerebrospinal fluid-contacting neurons in the rat spinal cord, a gamma-aminobutyric acidergic system expressing the P2X2 subunit of purinergic receptors, PSA-NCAM, and GAP-43 immunoreactivities: light and electron microscopic study. *J. Comp. Neurol.* 457, 159–174.
12. Fetcho, J.R. (1991). Spinal network of the Mauthner cell. *Brain Behav. Evol.* 37, 298–316.
13. Lacoste, A.M., Schoppik, D., Robson, D.N., Haesemeyer, M., Portugues, R., Li, J.M., Randlett, O., Wee, C.L., Engert, F., and Schier, A.F. (2015). A convergent and essential interneuron pathway for Mauthner-cell-mediated escapes. *Curr. Biol.* 25, 1526–1534.
14. Fetcho, J.R., and Faber, D.S. (1988). Identification of motoneurons and interneurons in the spinal network for escapes initiated by the Mauthner cell in goldfish. *J. Neurosci.* 8, 4192–4213.
15. Satou, C., Kimura, Y., Kohashi, T., Horikawa, K., Takeda, H., Oda, Y., and Higashijima, S. (2009). Functional role of a specialized class of spinal commissural inhibitory neurons during fast escapes in zebrafish. *J. Neurosci.* 29, 6780–6793.
16. Bagnall, M.W., and McLean, D.L. (2014). Modular organization of axial microcircuits in zebrafish. *Science* 343, 197–200.
17. Menelaou, E., and McLean, D.L. (2012). A gradient in endogenous rhythmicity and oscillatory drive matches recruitment order in an axial motor pool. *J. Neurosci.* 32, 10925–10939.
18. Myers, P.Z., Eisen, J.S., and Westerfield, M. (1986). Development and axonal outgrowth of identified motoneurons in the zebrafish. *J. Neurosci.* 6, 2278–2289.
19. Pietri, T., Manalo, E., Ryan, J., Saint-Amant, L., and Washbourne, P. (2009). Glutamate drives the touch response through a rostral loop in the spinal cord of zebrafish embryos. *Dev. Neurobiol.* 69, 780–795.
20. Knogler, L.D., and Drapeau, P. (2014). Sensory gating of an embryonic zebrafish interneuron during spontaneous motor behaviors. *Front. Neural Circuits* 8, 121.
21. Wells, S., Nornes, S., and Lardelli, M. (2011). Transgenic zebrafish recapitulating *tbx16* gene early developmental expression. *PLoS ONE* 6, e21559.
22. Warp, E., Agarwal, G., Wyart, C., Friedmann, D., Oldfield, C.S., Conner, A., Del Bene, F., Arrenberg, A.B., Baier, H., and Isacoff, E.Y. (2012). Emergence of patterned activity in the developing zebrafish spinal cord. *Curr. Biol.* 22, 93–102.
23. Kucenas, S., Soto, F., Cox, J.A., and Voigt, M.M. (2006). Selective labeling of central and peripheral sensory neurons in the developing zebrafish using P2X(3) receptor subunit transgenes. *Neuroscience* 138, 641–652.
24. Brustein, E., and Drapeau, P. (2005). Serotonergic modulation of chloride homeostasis during maturation of the locomotor network in zebrafish. *J. Neurosci.* 25, 10607–10616.
25. Freund, T.F., and Buzsáki, G. (1996). Interneurons of the hippocampus. *Hippocampus* 6, 347–470.
26. Jonas, P., Bischofberger, J., Fricker, D., and Miles, R. (2004). Interneuron Diversity series: Fast in, fast out—temporal and spatial signal processing in hippocampal interneurons. *Trends Neurosci.* 27, 30–40.
27. Freund, T.F., and Katona, I. (2007). Perisomatic inhibition. *Neuron* 56, 33–42.
28. Huang, Z.J., Di Cristo, G., and Ango, F. (2007). Development of GABA innervation in the cerebral and cerebellar cortices. *Nat. Rev. Neurosci.* 8, 673–686.
29. Mirat, O., Sternberg, J.R., Severi, K.E., and Wyart, C. (2013). ZebraZoom: an automated program for high-throughput behavioral analysis and categorization. *Front. Neural Circuits* 7, 107.
30. Dale, N., Roberts, A., Ottersen, O.P., and Storm-Mathisen, J. (1987). The development of a population of spinal cord neurons and their axonal projections revealed by GABA immunocytochemistry in frog embryos. *Proc. R. Soc. Lond. B Biol. Sci.* 232, 205–215.
31. Dale, N., Roberts, A., Ottersen, O.P., and Storm-Mathisen, J. (1987). The morphology and distribution of 'Kolmer–Agduhr cells', a class of cerebrospinal-fluid-contacting neurons revealed in the frog embryo spinal cord by GABA immunocytochemistry. *Proc. R. Soc. Lond. B Biol. Sci.* 232, 193–203.
32. Christenson, J., Alford, S., Grillner, S., and Hökfelt, T. (1991). Co-localized GABA and somatostatin use different ionic mechanisms to hyperpolarize target neurons in the lamprey spinal cord. *Neurosci. Lett.* 134, 93–97.
33. Jalalvand, E., Robertson, B., Wallén, P., Hill, R.H., and Grillner, S. (2014). Laterally projecting cerebrospinal fluid-contacting cells in the lamprey spinal cord are of two distinct types. *J. Comp. Neurol.* 522, 1753–1768.
34. Nair, A., Azatian, G., and McHenry, M.J. (2015). The kinematics of directional control in the fast start of zebrafish larvae. *J. Exp. Biol.* 218, 3996–4004.
35. Roberts, A., Hill, N.A., and Hicks, R. (2000). Simple mechanisms organise orientation of escape swimming in embryos and hatchling tadpoles of *Xenopus laevis*. *J. Exp. Biol.* 203, 1869–1885.
36. Deliagina, T.G., Beloozerova, I.N., Orlovsky, G.N., and Zelenin, P.V. (2014). Contribution of supraspinal systems to generation of automatic postural responses. *Front. Integr. Neurosci.* 8, 76.
37. Necker, R. (2006). Specializations in the lumbosacral vertebral canal and spinal cord of birds: evidence of a function as a sense organ which is involved in the control of walking. *J. Comp. Physiol. A Neuroethol. Sens. Neural Behav. Physiol.* 192, 439–448.
38. Meyer, M.P., and Smith, S.J. (2006). Evidence from in vivo imaging that synaptogenesis guides the growth and branching of axonal arbors by two distinct mechanisms. *J. Neurosci.* 26, 3604–3614.
39. Wen, H., and Brehm, P. (2005). Paired motor neuron-muscle recordings in zebrafish test the receptor blockade model for shaping synaptic current. *J. Neurosci.* 25, 8104–8111.
40. Zhu, P., Fajardo, O., Shum, J., Zhang Schäfer, Y.P., and Friedrich, R.W. (2012). High-resolution optical control of spatiotemporal neuronal activity patterns in zebrafish using a digital micromirror device. *Nat. Protoc.* 7, 1410–1425.